Generation of Raw Stepped-Frequency Waveform Echoes Using RCS Chamber Measurements

Jonathan E. Luminati, Air Force Institute of Technology
Todd B. Hale, Air Force Institute of Technology
Michael A. Temple, Air Force Institute of Technology
Michael J. Havrilla, Air Force Institute of Technology
Mark E. Oxley, Air Force Institute of Technology

Key Words: Stepped-Frequency Waveforms, HRR, ISAR, RCS

SUMMARY & CONCLUSIONS

Complicated microwave scattering characteristics of non-point targets are often examined using Radar Cross Section (RCS) chamber measurements. These measurements are designed to be waveform independent. Attempting to gather waveform dependent data on complex target responses typically requires a robust (and expensive) waveform generation and sampling capability beyond that of most RCS chambers. This paper introduces a technique to convert standard RCS chamber measurements into raw stepped-frequency waveform echoes. By controlling the construction and processing of these echoes, many waveform-dependent target effects can be examined. After demonstrating the validity of the proposed technique using both 1-D range profiles and 2-D Inverse Synthetic Aperture Radar (ISAR) images, the paper examines the effects of Linear Frequency Modulation (LFM) waveform filtering mismatches on an RCS chamber target.

1. INTRODUCTION

The improved resolution and increased waveform complexity of both High Range Resolution (HRR) and Synthetic Aperture Radar (SAR) systems promise to provide many new capabilities to both military and non-military radar systems. Yet the costs of designing and testing these systems can be prohibitive. To simplify the design process, targets are often assumed to be ideal point scatterers [1]. This assumption is central to one of the basic tools of waveform design and analysis, the ambiguity function $|\chi(\tau_d, f_d)|^2$ defined as

$$|\chi(\tau_d, f_d)|^2 = \left| \int_{-\infty}^{\infty} u(t) u^*(t + \tau_d) \exp(j2\pi f_d t) \mathrm{d}t \right|^2, \quad (1)$$

where $u(t)$ represents the transmitted waveform and the superscripted $*$ denotes the complex conjugate. This equation calculates the magnitude of the matched filter output power for a noise-free ideal point target, mismatched in range and frequency by time delay τ_d and Doppler shift f_d, respectively.

The point scatterer assumption also simplifies the simulation process. By assuming the radar's field-of-regard contains only isolated point targets, the composite radar echo from a given transmitted waveform can be found by superimposing several time-delayed replicas of the transmitted waveform. Each delayed replica is weighted according to one target's range and reflectivity characteristics [2].

Unfortunately, real targets do not typically respond as ideal point scatterers. They are often both complex (e.g., composed of more than one dominant scatterer within a resolution cell) and distributed (e.g., total target extent exceeds a resolution cell), especially for high resolution radars. Under these circumstances, a waveform's ambiguity function or auto/cross-correlation properties might not accurately reflect the response to actual targets, making it necessary to examine the performance of a given waveform on complex and/or distributed targets.

One popular way of studying real target scattering characteristics in a laboratory environment is through the use of Radar Cross Section (RCS) chambers. These chambers are designed to measure the response of a real target to user-defined illuminating waveforms. Through careful collection and processing, the RCS data represents the response of the target (which can be both complex and distributed) to far-field illumination in a free-space environment [3]. Using RCS chambers to make such measurements allows for significant cost and complexity savings over trying to take such measurements using operational systems in the field.

Many modern RCS chambers work by transmitting a series of relatively long, single-frequency pulses and measuring the target response at a predetermined range delay corresponding to the target center. The pulsewidth τ is made sufficiently long for the transmitted pulse to cover the entire target simultaneously. This requirement ensures the target response characteristics are identical to those of a Continuous Wave (CW) radar [3]. The CW illumination means only a single complex sample is necessary to represent the target response to a given frequency and orientation angle. Calculation of 1-D range profiles and 2-D Inverse SAR (ISAR) images is then accomplished using Fourier transforms and/or other related techniques [4].

Due in part to the CW sampling paradigm, most modern RCS chambers have limited arbitrary waveform generation capability. Furthermore, the filtered output data represents the target's spatial frequency response and is essentially waveform independent. This independence means that while RCS chambers

Report Documentation Page

Form Approved
OMB No. 0704-0188

1. REPORT DATE	2. REPORT TYPE	3. DATES COVERED
01 MAY 2005	**N/A**	**-**

4. TITLE AND SUBTITLE	5a. CONTRACT NUMBER
Generation of Raw Stepped-Frequency Waveform Echoes Using RCS Chamber Measurement	5b. GRANT NUMBER
	5c. PROGRAM ELEMENT NUMBER
6. AUTHOR(S)	5d. PROJECT NUMBER
	5e. TASK NUMBER
	5f. WORK UNIT NUMBER
7. PERFORMING ORGANIZATION NAME(S) AND ADDRESS(ES) **Air Force Institute of Technology**	8. PERFORMING ORGANIZATION REPORT NUMBER
9. SPONSORING/MONITORING AGENCY NAME(S) AND ADDRESS(ES)	10. SPONSOR/MONITOR'S ACRONYM(S)
	11. SPONSOR/MONITOR'S REPORT NUMBER(S)

12. DISTRIBUTION/AVAILABILITY STATEMENT
Approved for public release, distribution unlimited

13. SUPPLEMENTARY NOTES
See also ADM002017. Proceedings of the 2005 IEEE International Radar Conference Record Held in Arlington, Virginia on May 9-12, 2005. U.S. Government or Federal Purpose Rights License

14. ABSTRACT

15. SUBJECT TERMS

16. SECURITY CLASSIFICATION OF:			17. LIMITATION OF ABSTRACT	18. NUMBER OF PAGES	19a. NAME OF RESPONSIBLE PERSON
a. REPORT	b. ABSTRACT	c. THIS PAGE			
unclassified	**unclassified**	**unclassified**	**UU**	**6**	

can characterize the complicated scattering mechanisms of real targets, they have very limited capability for studying diverse waveform effects on these targets.

This paper proposes a technique for using RCS chamber spatial frequency data to generate high quality approximations of raw (unfiltered) time-domain waveform target echoes composed of Stepped-Frequency (SF) subpulses. With such data it then becomes possible to study the response of waveforms to complex and/or distributed targets without the added difficulty and expense of generating and sampling the true raw SF waveforms themselves.

2. STEPPED-FREQUENCY WAVEFORMS

SF waveforms are formed by concatenating a series of N single-frequency sinusoidal subpulses. Each subpulse has a duration τ_s giving the complete SF waveform a duration of $\tau = N\tau_s$. Each of the N subpulses has a unique frequency f_n. These frequencies are uniformly spaced by a frequency difference Δf and span a total 4.0 dB bandwidth of $B = N\Delta f$. Mathematically, the complete SF transmitted waveform $w_{TX}(t)$ can be written as

$$w_{TX}(t) = \sum_{n=0}^{N-1} \mathrm{rect}\left(t - n\tau_s\right) \exp(j2\pi f_n t), \tag{2}$$

where $\mathrm{rect}(\cdot)$ is defined as

$$\mathrm{rect}(t) = \begin{cases} 1 & : \quad 0 \le t < \tau_s \\ 0 & : \quad \text{otherwise.} \end{cases} \tag{3}$$

From Fourier transform theory, it is well known that finite subpulse duration effectively spreads the bandwidth of the individual subpulses. This effect determines the required relationship between B, τ, and N given by [5]

$$B\tau = N^2. \tag{4}$$

If $B < N^2/\tau$, subpulse energy bleeds outside the desired subpulse 4.0 dB bandwidth $B_s = \Delta f$. Conversely, if $B > N^2/\tau$, total bandwidth B becomes greater than the sum of the N subpulse bandwidths, leading to gaps in the frequency coverage and causing range aliasing artifacts.

Note that while frequency spacing is tightly controlled by (4), any subpulse frequency order is valid. By arranging the subpulse frequencies in a monotonically increasing or decreasing order, the SF waveform provides a good approximation to an LFM chirp. By randomizing the frequencies, a more noise-like frequency-hopped waveform is produced.

3. WAVEFORM GENERATION TECHNIQUE

Using the CW RCS chamber paradigm, the expected radar echo for a CW single-frequency waveform is simply an appropriately delayed copy of the transmitted waveform scaled by the complex In-phase and Quadrature (I/Q) sample measured in the RCS chamber. This observation is key to the waveform generation technique since an SF waveform is simply a collection of finite duration single-frequency subpulses. Provided the temporal extent of the target τ_t is much less than duration of a subpulse τ_s, the subpulse echo complex-valued amplitude should be essentially determined by the CW I/Q value measured in the standard data collection process.

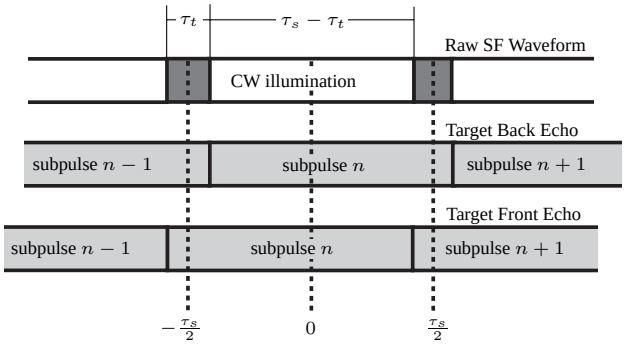

Figure 1: SF waveform generation principle. Horizontal axis is time. Bottom row denotes echo timing off target front (subpulse width τ_s). Middle row denotes echo timing off target back (target extent τ_t). Top row denotes raw SF waveform generated by the technique. White regions indicate where the single-frequency CW illumination assumption is valid.

Figure 1 illustrates this principle. The majority of the subpulse echo contains energy from the entire target and no other subpulses, indicating echo amplitude is determined by the CW I/Q sample measured during the standard data collection. The echo edges only contain energy from part of the target as well as echoes from adjacent subpulse frequencies, indicating the CW I/Q sample is not completely accurate in these regions. Note that the subpulse width τ_s is not determined by the true pulse width used in the RCS data collection but by (4).

Since the goal of the proposed technique is to produce an accurate raw SF waveform echo using only CW data, the percentage of time the CW assumption is valid relates directly to the accuracy of the waveform produced. To help quantify this accuracy, the variable γ is used, representing the percent of the raw SF wave for which the single-frequency CW illumination assumption is valid. It is determined by

$$\gamma = \begin{cases} 0 & : \quad \tau_s \le \tau_t \\ 1 - \frac{\tau_t}{\tau_s} & : \quad \tau_s > \tau_t \end{cases}, \tag{5}$$

where

$$\lim_{\tau_s \to \infty} \gamma = \lim_{\tau_t \to 0} \gamma = 1, \tag{6}$$

implying that for infinitely long subpulses or infinitesimally short targets, the CW illumination assumption is valid at all times.

For uniform spacing of subpulse frequencies and constant subpulse width, (4) can be used to show that

$$\Delta f = \frac{1}{\tau_s}. \tag{7}$$

Converting (7) into units of range with $r = ct/2$ gives

$$\Delta r_s = \frac{c\tau_s}{2} = \frac{c}{2\,\Delta f} = N\frac{c}{2B}, \tag{8}$$

where Δr_s is the range extent of a subpulse and c is the propagation velocity. Note that frequency spacing also determines the alias-free target range extent Δr thus

$$\Delta r = N\frac{c}{2B} = \Delta r_s, \tag{9}$$

indicating the ratio of subpulse width to target width is equal to

the frequency oversampling ratio[1], thereby determining γ.

Implementation of the proposed waveform generation technique begins by generating a digital copy of the raw SF waveform $w_{TX}(t)$ without incorporating any target information. The subpulses are ordered as desired to form the user-specified frequency hopping pattern. The RCS chamber data is incorporated into this transmitted waveform by superimposing the appropriate I/Q sample on each subpulse. This procedure allows the received target echo to be written from (2) as

$$w_{\mathrm{RX}}(t) = \sum_{n=0}^{N-1} A_n \mathrm{rect}\left(t - n\tau_s\right) \exp(j2\pi f_n t), \qquad (10)$$

where A_n represents the complex-valued I/Q sample at the frequency f_n. Equation (10) assumes the CW spatial frequency value measured by the RCS chamber radar is valid over the entire subpulse width τ_s. In reality, it is only valid over a region of length $\tau_s - \tau_t$, but this assumption is quite accurate for $\gamma \approx 1$. Note that a range (time) offset isn't necessary since the chamber processing references the I/Q samples to the target mount center.

4. 1-D VALIDATION: COMPLEX RANGE PROFILES

Before making use of the raw SF waveform echo model introduced in the previous section, it is necessary to verify its accuracy. This verification is accomplished by comparing range profiles produced via standard processing of the I/Q data to those produced by matched filtering the raw SF echoes generated using (10).

Due to the CW nature of the complex-valued I/Q samples, standard range profile generation is performed using an Inverse Fourier Transform (IFT)

$$\rho_{\mathrm{std}}(r) = \mathcal{F}^{-1}\left[A(k_r)\right], \qquad (11)$$

where $\mathcal{F}^{-1}$ is the IFT and $A(k_r)$ is the set of all I/Q samples at the given orientation angle as a function spatial frequency $k_r = 4\pi/\lambda$.

Calculation of the matched filtered range profile using the raw SF waveform is accomplished in a few simple steps. First, both the transmitted and received signals are multiplied by a phase correction term

$$w'_{\mathrm{TX}}(t) = w_{\mathrm{TX}}(t) \exp\left[-j2\pi \min\left\{f_n\right\} t\right], \qquad (12)$$

$$w'_{\mathrm{RX}}(t) = w_{\mathrm{RX}}(t) \exp\left[-j2\pi \min\left\{f_n\right\} t\right], \qquad (13)$$

where $\min\{f_n\}$ is the minimum frequency collected in the RCS chamber over $n \in \{0, ..., N-1\}$. This phase correction shifts the frequency band covered by the data to the range $0 \leq f_n \leq B$ and is necessary because of the inherent low-pass nature of digital IFT methods used to compute (11). Matched filtering of the signals in (12) and (13) is then performed in the frequency domain to give

$$\rho_{\mathrm{MF}}(r) = \mathcal{F}^{-1}\left\{\mathcal{F}\left[w'_{\mathrm{RX}}(r)\right] \mathcal{F}^{*}\left[w'_{\mathrm{TX}}(r)\right]\right\}, \qquad (14)$$

where $\mathcal{F}$ denotes a standard Fourier Transform (FT), the superscript $*$ takes the complex conjugate of the FT output, and the time t has been converted to range r using $r = ct/2$. The raw SF waveform echo in (10) is considered valid when

$$\rho_{\mathrm{std}}(r) \approx \rho_{\mathrm{MF}}(r). \qquad (15)$$

[1]The ratio of measured frequency spacing Δf to Nyquist frequency spacing.

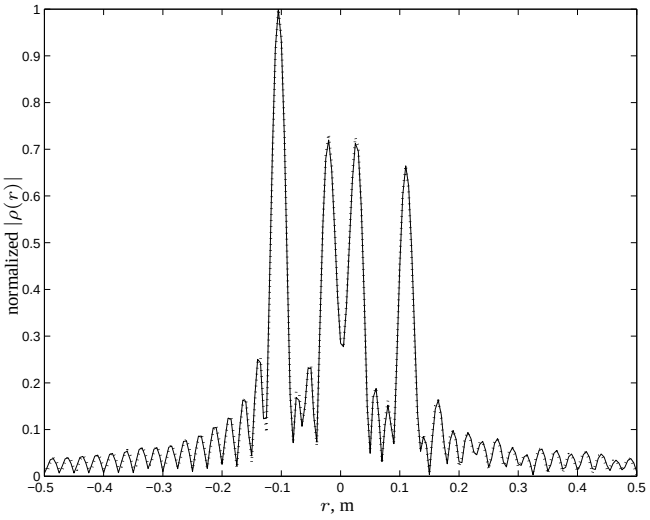

Figure 2: Comparison of $|\rho_{\mathrm{std}}(r)|$ (solid line) and $|\rho_{\mathrm{MF}}(r)|$ (dotted line) for a single range profile. Results are virtually identical.

To test waveform validity, data was collected on a distributed target consisting of four vertical wires, 9.5 cm tall, imbedded in a styrofoam block at the corners of a square with 15.2 cm sides. The radar used VV polarization and sampled the target response over $12 \leq f \leq 18$ GHz using $\Delta f = 30$ MHz and over azimuth angles from -45° to 45°, spaced by $0.45°$. This produced a square I/Q matrix with 201 complex-valued frequency samples at each of the 201 azimuth locations.

Figure 2 illustrates a comparison of normalized $|\rho_{\mathrm{std}}(r)|$ (solid line) and $|\rho_{\mathrm{MF}}(r)|$ (dotted line) results at an arbitrary azimuth angle. The subpulse frequency order was randomized to generate a noise-like frequency hopped SF waveform. The results are virtually identical across the entire target range.

Figure 3 illustrates a comparison of the phase for the two range profiles depicted in Fig. 2. The phases are essentially equal in the center of the target region (defined by the maximum target extent as $|r| < 11$ cm) and degrade somewhat away target center. This degradation is consistent with the understanding that the CW assumption validity is inversely proportional to target width.

To get a more statistical sense of the technique's validity, the magnitude and phase errors of $\rho_{\mathrm{MF}}(r)$ were calculated for each of the 201 azimuth samples. The mean values of these results were then computed to give the data shown in Figs. 4 and 5. To test the effect of Δf on technique accuracy, the range profiles were calculated using three different Δf values. The solid lines show results from using all 201 frequency samples ($\Delta f = 30$ MHz, $N = 201$). The dashed lines show results after decimating the frequency samples by a factor of two ($\Delta f = 60$ MHz, $N = 101$). The dotted lines show results after decimating the frequency samples by a factor of four ($\Delta f = 120$ MHz, $N = 51$). The target width (22 cm), combined with the three Δf values, gives γ values of 0.96, 0.91, and 0.84, respectively.

Figure 4 shows the mean error of $|\rho_{\mathrm{MF}}(r)|$. As expected, the

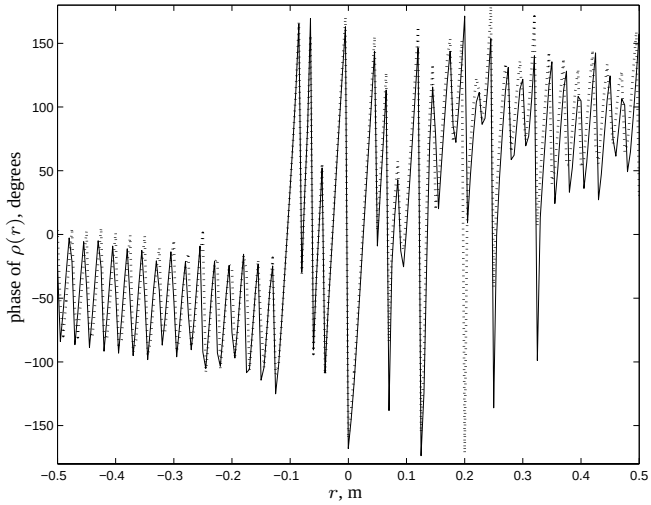

Figure 3: Comparison of $\rho_{\rm std}(r)$ (solid line) and $\rho_{\rm MF}(r)$ (dotted line) phases for a single range profile. Results are virtually identical near $r = 0$ and degrade as $|r|$ increases.

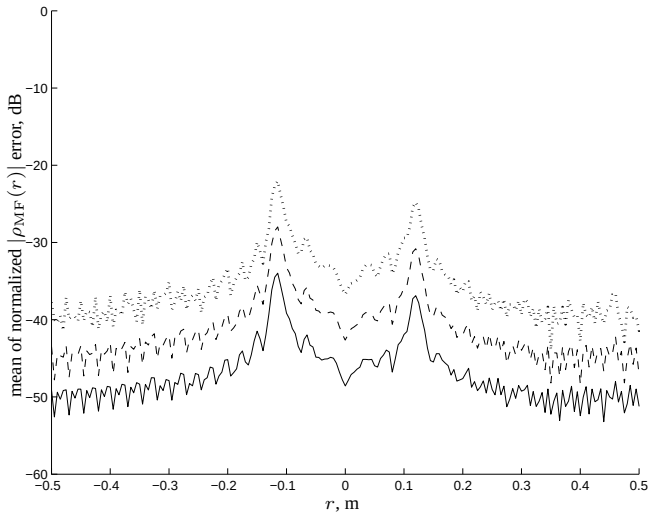

Figure 4: Mean of normalized $|\rho_{\rm MF}(r)|$ error over all 201 range profiles. Solid, dashed, and dotted lines denote $\Delta f = 30$, $\Delta f = 60$, and $\Delta f = 120$ MHz, respectively.

minimum errors, within the target extent, occur at $r = 0$ and rise as $|r|$ increases. The peak errors occur at roughly the maximum target extent and then fall rapidly. This decrease results from the lack of echo energy at large $|r|$. Also note the error gets worse as Δf increases, causing γ to decrease. In all cases, the worst case magnitude error is still quite small.

Figure 5 illustrates the mean phase error of $\rho_{\rm MF}(r)$. The phase errors are at a minimum near $r = 0$. The increase for $|r| > 0$ is relatively smooth within the target extent, but becomes more oscillatory when the range falls outside the target region. As Δf increases, both the minimum error and rate of error growth increase significantly.

The results presented in Figs. 4 and 5 clearly demonstrate the links between γ and SF waveform accuracy. Based on these results, a $\gamma \geq 0.9$ should be adequate for the given target. The criterion for this selection is that in many electromagnetics applications, phase errors are not deemed significant until they reach 22.5° [3][2]. By ensuring $\gamma \geq 0.9$ this requirement is met with reasonably high confidence.

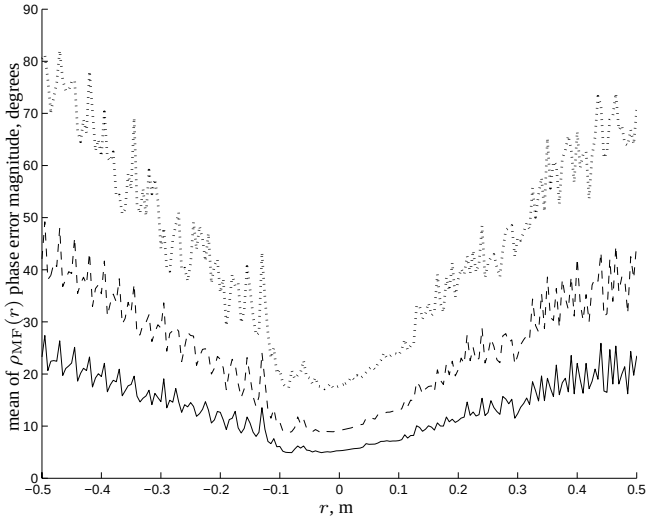

Figure 5: Mean of $\rho_{\rm MF}(r)$ phase error magnitude over all 201 range profiles. Solid, dashed, and dotted lines denote $\Delta f = 30$, $\Delta f = 60$, $\Delta f = 120$ MHz, respectively.

5. 2-D VALIDATION: ISAR IMAGERY

While 1-D range profiles may be sufficient for HRR applications, the proposed SF waveform generation technique would be much more valuable if it was also applicable to 2-D ISAR imaging. ISAR imaging takes a collection of range profiles from many different target look-angles and coherently combines them to produce 2-D target images. The ISAR images shown in this paper were produced using a standard (global) back-projection algorithm [6, 7]. Back-projection algorithms work by spreading each complex-valued 1-D range profile across a 2-D image plane and then coherently summing these planes to produce the final image.

Figure 6 illustrates the unwindowed ISAR image obtained using standard range profiles, plotted on a 50.0 dB log scale. The four vertical wires are clearly visible. Sparse data in the 2-D spatial frequency domain causes the bow-tie shaped sidelobes emanating from each wire [8].

Figure 7 is the image which results from processing raw SF waveforms generated from the I/Q data samples, decimated by a factor of two ($\gamma = 0.91$). As desired, the resulting image is virtually indistinguishable from Fig. 6.

6. LFM WAVEFORM EFFECTS

Having demonstrated the validity of the proposed waveform generation process for both 1-D and 2-D data processing, it is now possible to apply the technique to some of the problems outlined in the introduction. This section examines both the ambiguity and cross-correlation properties of LFM waveforms as applied to the distributed target introduced in Sections 4. and 5. All data in this section has been decimated by a factor of two,

[2]This value is often used to define the tolerable phase error for applying the far-field assumption in electromagnetic wave propagation applications.

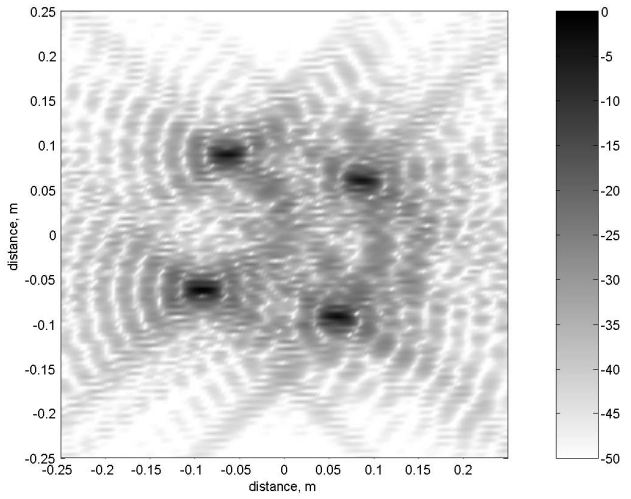

Figure 6: ISAR image generated using traditional range profiles.

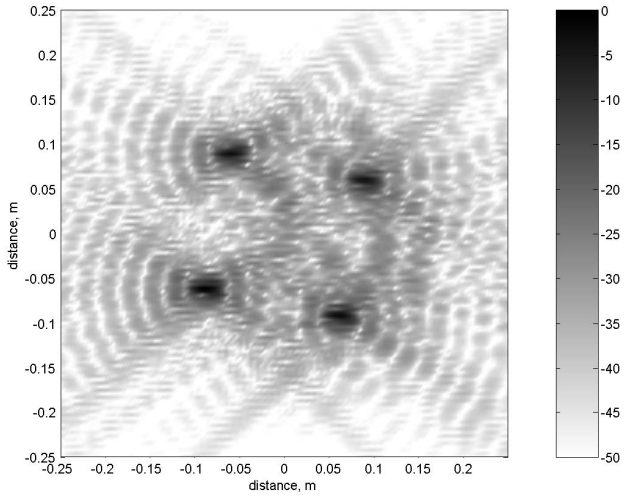

Figure 7: ISAR image generated using SF waveforms with random subpulse frequency order.

implying $\Delta f = 60$ MHz, $N = 101$, and $\gamma = 0.91$.

One reason for the prevalence of LFM waveforms is the fact that they exhibit roughly uniform gain over a wide range of Doppler frequencies, allowing HRR systems the ability to detect targets across a large Doppler band. Unfortunately, LFM waveforms also suffer from an effect known as range-Doppler coupling, (i.e., large target Doppler shifts cause an apparent offset in target range) [5]. Using the proposed SF waveform generation technique, this effect can be seen in the range profiles of complex and/or distributed targets.

Figure 8 shows the result of applying a Doppler shift of $f_d = 600$ kHz to the range profile of Fig. 2. This application is performed by adding an additional exponential phase term to (13). The range profile is then calculated using (14). The dotted line shows the true range profile (Fig. 2), while the solid line indicates the range profile calculated using the Doppler shifted target echo. The central region of the profile is shifted by an

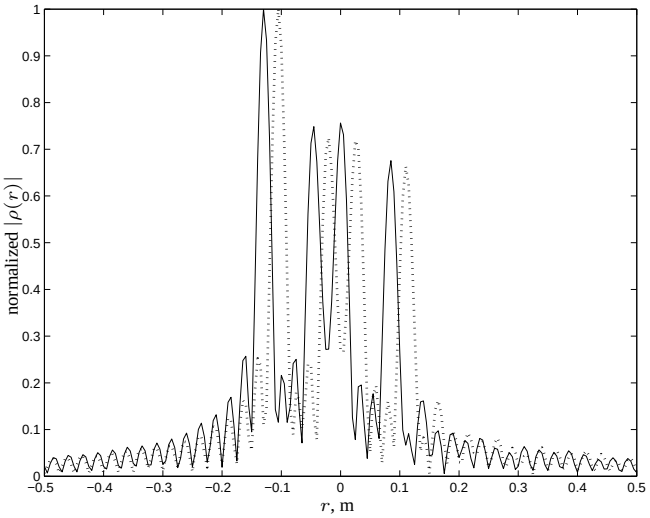

Figure 8: Range-Doppler coupling effect of an LFM upchirp on 1-D range profile. Dotted line shows the true range profile calculated with a matched filter. Solid line shows range profile generated by a mismatch of $f_d = 600$ kHz.

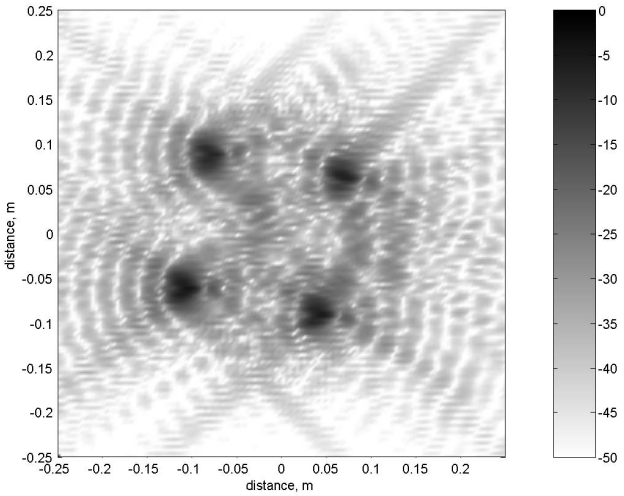

Figure 9: Range-Doppler coupling effect of an LFM upchirp on 2-D ISAR image.

amount

$$\delta r = \frac{\tau c}{2B} f_d, = 2.55\,\mathrm{cm} \tag{16}$$

in accordance with the linear range-Doppler coupling relationship.

Using this Doppler offset on each range profile, it becomes possible to generate an ISAR image of the Doppler shifted target. This result is shown in Fig. 9. Comparing this to the image of the zero Doppler target (Fig. 7) shows that the range-Doppler coupling has caused some defocusing of the ISAR target. This effect is primarily caused by changing target orientation angle throughout the RCS data collection.

A second interesting application of the proposed waveform generation technique is for testing waveform cross-correlation properties. One common limitation with HRR systems is their inability to provide a large unambiguous range r_u. One tech-

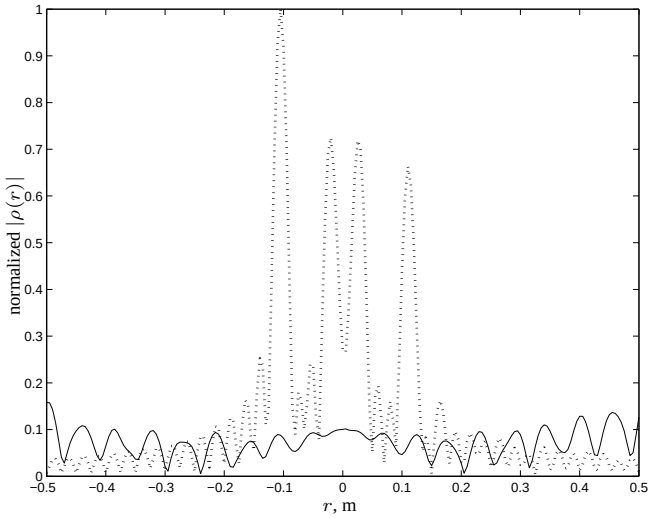

Figure 10: Cross-correlation effects on 1-D range profile. Dotted line shows range profile generated by matched filtering an LFM upchirp. Solid line shows range profile generated by mismatched filtering with an LFM downchirp.

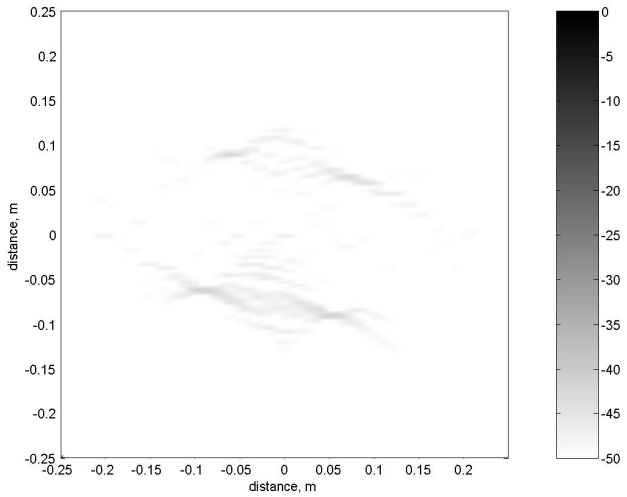

Figure 11: Cross-correlation effects on 2-D ISAR image. Mismatched filtering performed on LFM upchirp data using LFM downchirp reference.

nique for increasing r_u is to transmit an alternating sequence of LFM upchirped and downchirped waveforms. Assuming these two waveforms are orthogonal, this technique essentially doubles r_u. However, these two waveforms are not truly orthogonal, meaning some residual target energy remains after matched filtering with the incorrect waveform. Using the SF waveform generation technique, it is possible to examine the validity of the orthogonality assumption for realistic HRR/ISAR targets.

Figure 10 illustrates the result of applying an LFM downchirp filter to an LFM upchirp target echo. The true matched filtered range profile (Fig. 2) is shown as the dotted line, while the mismatched result is indicated by the solid line. The peak target response has been reduced by about a factor of 10 (-20.0 dB).

Figure 11 shows the ISAR image generated from the coherent combination of all 201 range profiles. While the four wires do appear at the right image coordinates, the peak pixel value has fallen dramatically. The peak value results from the non-coherent combination of the individual mismatch filtered range profiles. Assuming the non-coherent target energy adds as the square root of the range profiles, an expected peak image value $(\max[f(x,y)])$ can be estimated as

$$\max[f(x,y)] = 20\log_{10}\left(\frac{0.1}{\sqrt{201}}\right) \approx -43.0, \qquad (17)$$

where the expected peak value of the mismatch filtered range profile is about 0.1 (taken from Fig. 10). The prediction in (17) is very close to the true image peak of -41.0 dB.

7. CONCLUSION

This paper introduced a technique for taking waveform independent CW RCS chamber measurements and producing raw SF waveform target echoes. After validating the technique with one and two-dimensional data, the technique was used to study LFM waveform effects on a distributed RCS chamber target. With the proposed capability it is possible to examine the effects of diverse waveforms and processing methods on complex and/or distributed targets without the added difficulty or expense of complicated waveform generation and sampling.

REFERENCES

[1] D. A. Ausherman, A. Kozuma, J. L. Walker, H. M. Jones, and E. C. Poggio, "Developments in radar imaging," *IEEE Transactions on Aerospace and Electronic Systems*, no. 4, pp. 363–400, July 1984.

[2] M. Soumekh, *Synthetic Aperture Radar Signal Processing*. New York, NY: John Wiley & Sons, Inc., 1999.

[3] E. F. Knott, J. F. Shaeffer, and M. T. Tuley, *Radar Cross Section*, 2nd ed. Norwood, MA: Artech House, 1993.

[4] W. G. Carrara, R. S. Goodman, and R. M. Majewski, *Spotlight Synthetic Aperture Radar: Signal Processing Algorithms*. Norwood, MA: Artech House, 1995.

[5] M. I. Skolnik, *Introduction to Radar Systems*, 3rd ed. Boston, MA: McGraw Hill, 2001.

[6] D. C. Munson Jr., J. D. O'Brian, and W. K. Jenkins, "A tomographic formulation of spotlight-mode synthetic aperture radar," *Proceedings of the IEEE*, vol. 71, no. 8, pp. 917–925, August 1983.

[7] A. F. Yegulalp, "Fast backprojection algorithm for synthetic aperture radar," in *The Record of the 1999 IEEE Radar Conference*, 1999, pp. 60–65.

[8] J. E. Luminati and W. Wood, "Fourier transform and back-projection methods of SAR/ISAR imaging using circumscribed processing regions," in *20th Annual Review of Progress in Applied Computational Electromagnetics*. Syracuse, NY: ACES, 2004.

"The views expressed in this article are those of the author(s) and do not reflect official policy of the United States Air Force, Department of Defense or the U.S. Government."